Iron limitation in the Western Interior Seaway during the Late Cretaceous OAE 3 and its role in phosphorus recycling and enhancing organic matter preservation

Allyson Tessin[1*], Nathan D. Sheldon[1], Ingrid Hendy[1], and Anthony Chappaz[2, 3]

[1]Department of Earth and Environmental Sciences, University of Michigan

[2]Institute for Great Lakes Research, Central Michigan University

[3]Department of Earth and Atmospheric Sciences, Central Michigan University

*Corresponding Author: atessin@umich.edu

Abstract

The sedimentary record of the Coniacian-Santonian Oceanic Anoxic Event 3 (OAE 3) in the North American Western Interior Seaway is characterized by a prolonged period of enhanced organic carbon (OC) burial. This study investigates the role of Fe in enhancing organic matter preservation and maintaining elevated primary productivity to sustain black shale deposition within the Coniacian-Santonian-aged Niobrara Formation in the USGS #1 Portland core. Iron speciation results indicate the development of a reactive Fe limitation coeval with reduced bioturbation and increased organic matter preservation, suggesting that decreased sulfide buffering by reactive Fe may have promoted enhanced organic matter preservation at the onset of OAE 3. An Fe limitation would also provide a feedback mechanism to sustain elevated primary productivity through enhanced phosphorus recycling. Additionally our results demonstrate inconsistencies between Fe-based and trace metal redox reconstructions. Iron indices from the Portland core indicate a single stepwise change, whereas the trace metal redox proxies indicate fluctuating redox conditions during and after OAE 3. Using Fe speciation to reconstruct past

redox conditions may be complicated by a number of factors, including Fe sequestration in diagenetic carbonate phases and efficient sedimentary pyrite formation in a system with limited Fe supply and high levels of export production.

Introduction

Iron availability in marine systems can significantly influence organic carbon (OC) accumulation in sediments by affecting rates of both primary productivity and organic matter preservation. In the modern ocean, increased Fe delivery or "fertilization" is known to enhance primary productivity in high nutrient, low chlorophyll regions (e.g. Boyd et al., 2000). In sediments, the availability and early diagenesis of Fe are known to play complex roles in OC accumulation by inducing changes in C, P, and S cycling (Canfield, 1989; Raiswell and Canfield, 1996). For example, Meyers (2007) outlined the role of Fe in the "sulfide buffer and phosphorus trap hypothesis," where reactive Fe minerals (especially Fe (oxyhydr)oxides) act to buffer sulfide buildup within porewaters through formation of Fe-sulfide mineral phases (FeS, FeS_2). Once all available reactive Fe is sulfidized, free sulfide accumulates in porewaters, which promotes P recycling in the absence of Fe (oxyhydr)oxides and reduces bioturbation and organic matter oxygen exposure time (Canfield, 1989; Raiswell and Canfield, 1996; Meyers, 2007; Tribovillard et al., 2015).

As some of the most dramatic examples of OC burial in the geologic record, Mesozoic Oceanic Anoxic Events (OAEs) provide unique opportunities for studying OC burial processes as each event varied in duration and geographic extent. The Cenomanian-Turonian OAE 2, for example, is characterized by widespread black shale deposition (Schlanger et al., 1987; Tsikos et al., 2002), and a distinctive and relatively short-lived (~600 ka: Sageman et al., 2006) positive

carbon isotope excursion (Arthur et al., 1987; Jenkyns, 2010). In contrast, OC-rich sedimentation during the Coniacian-Santonian OAE 3 was restricted to the equatorial Atlantic and adjacent continental shelves and seaways (e.g., März et al., 2008; Locklair et al., 2011; Wagreich, 2012), including the North American Western Interior Seaway (WIS). Due to the long duration (>3 Myrs) and higher rates of OC burial in some locations as compared to OAE 2, OAE 3 represents an important perturbation to the global carbon cycle. Irrespective of its exact geographic extent, OC burial during OAE 3 was elevated, widespread, and prolonged, and must have required internal oceanic feedback mechanisms.

This study investigates Fe speciation before, during and after OAE 3 in the WIS to understand its role in prolonged OC burial. A comparison of these results with S concentrations and previously published records of bioturbation (Savrda, 1998) and organic matter quality (Tessin et al., 2015) is used to assess how fluctuations in Fe availability can affect "sulfide buffering" and OC preservation, particularly at the onset of enhanced OC burial. Evolution of Fe speciation is also compared to TOC/P and P/Al ratios to evaluate how changes in Fe chemistry affected "P trapping" before, during, and after OAE 3. Finally, comparison of Fe speciation with redox sensitive trace metals provides a opportunity to test whether Fe-based redox reconstructions are supported by other redox proxies in highly productive sedimentary systems where pyrite formation may be Fe limited.

Background

Western Interior Seaway

During maximum transgression, the WIS extended from the Gulf of Mexico to the Arctic Ocean and from central Utah to central Iowa (Fig. 1). The sedimentary record of the WIS

70 includes episodic deposition of OC-rich shales and chalks, including those recorded during the
71 two maximum transgressions, the Greenhorn and the Niobrara Transgressions. The Niobrara
72 Formation was deposited during the latter transgression from the Late Turonian to the Early
73 Campanian (Scott and Cobban, 1964; Locklair et al., 2011) and is formally divided into two
74 members: the basal Fort Hays Limestone and the overlying Smoky Hill Chalk (Fig. 1). Previous
75 research has identified OAE 3 in the Smoky Hill Chalk based on a positive $\delta^{13}C$ excursion and
76 elevated OC concentrations (e.g. Locklair et al., 2011; Tessin et al., 2015).
77 Paleontological and sedimentary evidence indicates that in western Kansas and central
78 Colorado, the Fort Hays was initially deposited in water depths of 15–50 m and that the water
79 column progressively deepened to water depths of 150–300 m during Smoky Hill deposition
80 (Hattin, 1982). The focus of this study, the USGS Portland core, was located in the deepest
81 portion of the WIS during the Late Cretaceous (Fig 1; Sageman and Arthur, 1994). During
82 maximum transgression, the influx of Tethyan water from the south may have delivered
83 nutrients, including reactive Fe into the WIS (e.g. Meyers et al., 2005). Other sources of Fe and
84 nutrients to the seaway include continental runoff from the Sevier Highlands (e.g. Flögel et al.,
85 2009) and volcanic ash falls, which are recorded as numerous bentonite layers.
86
87 *Trace metal and iron redox proxies*
88 Trace metal concentrations in ancient sediments and rocks allow for the reconstruction of
89 marine redox conditions (Tribovillard et al., 2006). Cadmium and zinc accumulate in sediments
90 under sulfidic conditions. Cadmium exhibits a nutrient-like behavior and is delivered to
91 sediments with OM (Piper and Perkins, 2004). Zinc is delivered to the sediments via organic acid
92 complexes or through adsorption on Fe-Mn oxyhydroxides (Fernex et al., 1992; Algeo and

93 Maynard, 2004). During early diagenesis, Cd and Zn are released to porewaters from organic
94 matter and are authigenically enriched in sediments as CdS and ZnS in the presence of free
95 sulfide (Huerta-Diaz and Morse, 1992). Sedimentary Mo accumulation is thought to require a
96 threshold concentration of H_2S for molybdate to be transformed to the particle reactive
97 thiomolydbate (i.e. the thiomolybdate switch) and subsequently scavenged by OM and Fe – S
98 mineral phases (Erickson and Helz, 2000; Chappaz et al., 2014). Thus, more sulfidic conditions
99 are thought to be required for Mo accumulation than for Cd and Zn accumulation. Rhenium also
100 accumulates in reducing sediments but unlike Mo, Zn, and Cd, sedimentary enrichment is not
101 thought to require the presence of free H_2S (Crusius et al., 1996).
102 Iron speciation has also been used as a redox proxy to distinguish oxic, ferruginous or
103 euxinic conditions in ancient black shales. This approach is based on the observation that Fe,
104 particularly highly reactive Fe (Fe_{HR}), is enriched in sediments deposited beneath an anoxic
105 water column (e.g. Raiswell and Anderson, 2005; Lyons and Severmann, 2006). Therefore,
106 Fe_T/Al ratios of >0.5 and Fe_{HR}/Fe_T of >0.38 are indicative of an anoxic water column (e.g.
107 Poulton and Canfield, 2005; Lyons and Severmann, 2006). Studies of modern euxinic basins
108 (e.g. Black Sea, Cariaco Basin) have identified the source of Fe enrichment in anoxic basins as
109 reactive Fe shuttled from suboxic shallow shelf sediments and subsequently precipitated within
110 the water column in the deeper euxinic basin (Lyons and Severmann, 2006; Severmann et al.,
111 2010). The ratio of Fe_{py}/Fe_{HR} can be further used to distinguish between euxinic and non-euxinic
112 anoxic systems because significant sulfidization of the Fe_{HR} pool (>0.7–0.8) has been used to
113 indicate the presence of dissolved H_2S in the water column (Raiswell and Canfield, 1998; März
114 et al., 2008; Poulton and Canfield, 2011; Poulton et al., 2015).

115 Certain factors, including basin geometry, high sedimentation rates, and low Fe export
116 efficiency from the shelves, are known to complicate the interpretation of Fe-speciation results
117 by decreasing Fe_{HR}/Fe_T and Fe_{py}/Fe_{HR} values (Raiswell and Canfield 1998; Anderson and
118 Raiswell 2004; Raiswell and Anderson 2005; Lyons and Severmann, 2006). These complications
119 are generally thought to obscure the signal of anoxic conditions rather than erroneously indicate
120 anoxic/euxinic conditions. Basin geometry, in particular the shelf to basin ratio, is of interest in
121 the current study because "shelf" settings are defined as <200 m water depth, which means that
122 most, if not all, of the WIS is considered to be a shelf and not deep basin setting.
123
124 Methods and materials
125 The USGS #1 Portland core was drilled and continuously cored near Cañon City, CO
126 (Dean and Arthur, 1998). The 75-m thick Late Cretaceous Niobrara Formation section of the
127 Portland core was sampled at 0.5 m resolution at the USGS Core Research Center in Denver, CO
128 (Fig. 1). Chemostratigraphy for the core is based on carbon isotope and total organic carbon
129 records presented in Tessin et al. (2015), which was used to identify pre-OAE, OAE, and post-
130 OAE intervals. In Fig. 1, the three defined intervals from Tessin et al. (2015) are further divided.
131 The pre-OAE Interval (Interval 1) has been partitioned into Interval 1a, which includes the Fort
132 Hays Limestone and Interval 1b, which includes the lower shale limestone member of the Smoky
133 Hill Chalk (Scott and Cobban, 1964). The OAE Interval (Interval 2) is divided into 2a, 2b, and
134 2c based on previously published total organic carbon (TOC) values (Tessin et al., 2015; Fig. 1).
135 Intervals 2a and 2c are defined by TOC values >3%. The post-OAE Interval (Interval 3) was not
136 subdivided.
137 Samples analyzed for bulk elemental concentrations (Al, Fe, S, P, Mo, Re, Cd, and Zn)

were ground to <75 μm and homogenized in an alumina shatterbox to minimize trace element contamination. Analyses were completed at ALS Laboratories in Vancouver, BC. Whole rock samples were digested with perchloric, hydrofluoric, nitric, and hydrochloric acids. Concentrations were determined by inductively coupled plasma-atomic emission spectrometry (ICP-AES) and inductively coupled plasma-mass spectrometry (ICP-MS). GBM908-10, GBM908-5, OREAS 90 and MRGeo08 standards were used to verify elemental concentrations. Accuracy and precision are reported in Supplemental Table 1.

Sequential iron extractions were completed following Poulton and Canfield (2005), and pyrite Fe extractions following Canfield et al. (1986). The pyrite fraction is stoichiometrically determined following precipitation of chromium reducible sulfide as ZnS. Iron phases measured are outlined in Table 1. Carbonate-associated Fe (Fe_{carb}), magnetite Fe (Fe_{mag}), and Fe (oxyhydr)oxides (Fe_{ox}) are considered highly reactive (HR) because these phases react with sulfide on timescales of months to years (Poulton and Canfield, 2005). The Fe_{HR} pool also includes pyrite Fe (Fe_{py}), which represents Fe that has reacted with sulfide in the water column or during early diagenesis in the sediments (Raiswell and Canfield, 1998; Poulton and Raiswell, 2002). The Fe_{HR} pool is thus defined as $Fe_{carb} + Fe_{ox} + Fe_{mag} + Fe_{py}$ and poorly and non-reactive Fe ($Fe_{NR/PR}$) is calculated as $Fe_T - Fe_{HR}$. Concentrations of Fe_{carb}, Fe_{ox}, and Fe_{mag} were measured on ICP-MS (Thermo iCAP Q) within the STARLAB at Central Michigan University. Analytical precision and accuracy, determined from replicate analyses (n = 21) of a certified standard (SCP Science) were better than 5%. Calculated pyrite Fe concentrations generally replicated with <5% precision. All geochemical data discussed in this paper are archived in Pangaea (www.pangaea.de).

Results

Iron

The different Fe phases identified by sequential extractions and pyrite Fe measurement are plotted in Fig. 2. Carbonate-associated Fe (Fe_{carb}) is generally elevated during Interval 1, with concentrations up to 0.2 wt. %, whereas during Intervals 2 and 3, Fe_{carb} concentrations are consistently < 0.05 wt. %. Iron (oxyhydr)oxides (Fe_{ox}) consistently accounts for between 0.01–0.1 wt. % throughout the Portland record. Magnetite-associated Fe (Fe_{mag}) is generally low but varies throughout the three intervals. During Interval 1, Fe_{mag} concentrations range from 0.01–0.07 wt. %. Concentrations of Fe_{mag} are consistently <0.01 wt. % during Interval 2 and range between 0.02–0.04 wt.% during Interval 3. Pyrite-associated Fe (Fe_{py}) increases notably leading into Interval 2 to concentrations of between 0.2–1.1 wt.%. During Intervals 2 and 3, an average of 88% of Fe_{HR} is in the form of Fe_{py}.

The Fe_T/Al values are the most variable and elevated during Interval 1, with values ranging from 0.07 to 1.60 (Fig. 2). During Intervals 2 and 3, Fe_T/Al values average 0.51 and 0.46, respectively. Values of Fe_T/Al are elevated during Intervals 2a and slightly elevated during Interval 2c. Values of Fe_{HR}/Fe_T range between 0.36 and 0.88 with an average value of 0.60 throughout the record. The lowest values (0.12 and 0.33) of Fe_{py}/Fe_{HR} occur during Interval 1a. Values of Fe_{py}/Fe_{HR} increase abruptly in Interval 1b with values ranging between 0.71 and 0.93 for the remainder of the record.

Trace metals

Trace metal/Al ratios are plotted as ppm (Mo, Cd, Zn) or ppb (Re) to weight % ratios and compared to previously published Mo and TOC concentrations from Tessin et al. (2015) in Fig.

3. The records of Mo concentrations and Mo/Al exhibit similar patterns throughout the Portland core, and generally follow the TOC record (Fig. 3). Interval 1 is characterized by low Mo concentrations (an average of 0.3 ppm) and Mo/Al ratios (an average of 0.2). Interval 2 exhibits the most variable Mo and Mo/Al values, with two peak periods of elevated Mo concentrations during Intervals 2a and 2c separated by low concentrations during Interval 2b. During Interval 3, Mo concentrations and Mo/Al values become more stable, ranging from 8.5–36 ppm and 1.9–10.8, respectively. The record of Mo/TOC exhibits similar trends to the Mo and Mo/Al record, with the lowest values recorded during Interval 1 (1.0). Within Interval 2, Mo/TOC concentrations are elevated during Intervals 2a and 2c, with low values recorded during Interval 2b. However, unlike the Mo and Mo/Al records, Mo/TOC values within Interval 3 are elevated and variable, ranging from 2.8–40.9.

Rhenium, Cd, and Zn behave similarly to Mo in the Portland core (Fig 3). Throughout Interval 1, Re/Al, Cd/Al, and Zn/Al values are generally low (an average of 3.8, 0.08, and 27, respectively). The highest Re/Al, Cd/Al, and Zn/Al values occur during Intervals 2a and 2c, whereas Interval 2b exhibits values similar to Interval 1. During Interval 3, values remain elevated and range between 7–85, 0.4–3.1, and 7–91, respectively.

Sulfur and Phosphorus

Sulfur results are compared to previously published TOC, bioturbation, and Rockeval results from Tessin et al. (2015) and Savrda (1998) in Fig. 4. Bioturbation derived Interpreted Oxygenation Curves (IOC) from Savrda (1998) are based on the vertical distribution of laminites and oxygen-related ichnocoenoses. The IOC record has been smoothed by integrating data to 0.5 m resolution to match the resolution of the geochemical data. IOC values generally decrease

throughout Interval 1, with the lowest values recorded within Interval 2, indicating reduced bioturbation during the OAE (Savrda, 1998). Hydrogen and oxygen index values, produced through RockEval pyrolysis, are proxies for the hydrogen- and oxygen-richness of organic matter. Hydrogen index values are markedly elevated in Interval 2, as compared to Interval 1, highlighting an increase in the hydrogen-richness of organic matter. Conversely, oxygen index values are elevated in Interval 1 as compared to Interval 2, indicating a decrease in the oxygen-richness of organic matter (Tessin et al., 2015).

Weight % ratios of TS/Al indicate increasing S accumulation within the sediments throughout the record (Fig 4). During Interval 1, TS/Al averages 0.13 compared to an average of 0.51 and 0.38 during Intervals 2 and 3. Excess S/TS records (calculated as (TS-CRS)/TS) illustrate that between 13 and 44% of TS is non-CRS (Fig 5). Due to low concentrations of S and CRS in samples between 58 and 78 m in the core, errors on S_{excess}/TS increase but values are near 0%.

Phosphorus values are plotted as P/Al and TOC/P ratios in Figure 5. Trends in P geochemistry are based on total P and rather than organic or reactive P because it has been observed that P speciation records can be significantly altered by sample handling and diagenesis and that P_T/Al and TOC/P are the most reliable records of changes in P geochemistry in black shales (Algeo and Ingalls, 2007; Kraal et al., 2010). Calculations of P/Al ratios are shown as weight % ratios, while TOC/P values are calculated as molar ratios. During Interval 1, P/Al are highly variable, ranging between 0.009 and 0.170, with an average value of 0.04. During Intervals 2 and 3, P/Al values become less variable and average 0.025 and 0.018, respectively. TOC/P values are low throughout Interval 1, with an average molar ratio of 15. Molar ratios of

TOC/P range between 26 and 306 during Interval 2. During Interval 3, TOC/P molar ratio values stabilize with an average value of 99.

Discussion

Fe speciation and limitation

Comparison of Fe speciation and trace metal concentrations throughout the Portland record suggests that changes in Fe speciation and abundance are decoupled from redox conditions. During Interval 1a, the Fe_T/Al record exhibits significant variability (Fig. 2). Elevated Fe_T/Al (>1) and Fe_{HR}/Fe_T ratios (>0.38) both indicate sedimentary Fe enrichments. Samples enriched in Fe_{HR} are characterized by low Al_T (0.29–0.37 wt. %) and Fe_T (0.43–0.5 wt. %) concentrations, as well as high carbonate concentrations (94.8–96.7 wt. %; SI Table 2). While elevated Fe_T/Al and Fe_{HR}/Fe_T ratios could be interpreted as an indicator of periodic deposition under an anoxic water column, this interpretation is inconsistent with trace metal results. No enrichments in trace metals (Mo, Re, Cd, or Zn) are observed during Interval 1 (Fig. 3). This interval is also characterized by significant bioturbation and the presence of benthic macrofossils, both of which support well-oxygenated conditions (Savrda, 1998).

It has been shown in modern, carbonate-rich sediments that anomalously high Fe_T/Al values can occur when Fe_T is <0.5 wt. % due to incorporation of Fe^{2+} from anoxic porewaters into early diagenetic carbonate cements (Clarkson et al., 2014). Samples in the Portland core with <0.5 wt. % Fe, generally exhibit elevated Fe_T/Al ratios (>1) and have large contributions of carbonate-associated Fe (>40% of total Fe), whereas carbonate-associated Fe comprises less than 8% of total Fe in samples with >1 wt. % Fe (Fig. 2). The significant increase in Fe_{carb} suggests early diagenetic transformations of Fe within the sediments and pyrite formation limited by

252 sulfide supply (Raiswell et al., 2011). The latter is also supported by the S excess/TS data,
253 showing that all available sulfide has been sequestered into pyrite. Our results agree with the
254 modern compilation of Clarkson et al. (2014) that suggests that Fe speciation from carbonate-
255 rich samples <0.5 wt. % Fe may not accurately record redox conditions.

256 During Interval 1b, Fe_{py}/Fe_{HR} values increase abruptly and remain elevated throughout
257 the remainder of the record, suggesting efficient sulfidization of reactive Fe preceding, during
258 and after the OAE (Fig. 2). This transition marks a shift from sulfide limited to reactive Fe
259 limited pyrite formation in WIS sediments. Ratios of Fe_{HR}/Fe_T consistently falling above the
260 anoxic threshold value of 0.38 and elevated Fe_{py}/Fe_{HR} values suggest water column precipitation
261 of Fe^{2+} via pyrite formation under euxinic conditions preceding, during, and after the OAE (Fig.
262 2). However, persistent euxinia is inconsistent with trace metal distributions and biotic evidence,
263 which indicate fluctuating redox conditions (Savrda, 1998). Redox sensitive trace metals (Mo,
264 Re, Cd, and Zn) all exhibit consistent patterns throughout the Portland record, wherein trace
265 metal accumulations track TOC concentrations. In particular, during Intervals 1b and 2b, low
266 trace metal concentrations indicate relatively well-oxygenated conditions, despite consistently
267 elevated Fe_{py}/Fe_{HR}. Additionally, Intervals 1b and 2b are associated with increased bioturbation,
268 which is inconsistent with persistent euxinia (Savrda, 1998). Conversely, during Intervals 2a and
269 2c, elevated Mo, Cd, Re, and Zn concentrations and dominantly laminated (not bioturbated)
270 sediments (Savrda, 1998) support the presence of euxinic conditions indicated by elevated
271 Fe_{py}/Fe_{HR} and Fe_{HR}/Fe_T ratios.

272 The differences between Fe_{py}/Fe_{HR} and Mo, two proxies for euxinia, are highlighted in
273 Fig. 6. Based on modern observations, Scott and Lyons (2012) proposed that Mo enrichment
274 levels can be correlated with specific redox conditions: oxic (up to 2 ppm), anoxic (chemocline

275 located within sediment, 2–25 ppm), intermittently euxinic conditions (chemocline located
276 within water column, 25–100 ppm), and permanently euxinic (>100 ppm). However, Mo
277 concentrations >25 ppm are only recorded within Intervals 2a and 2c, despite Fe_{py}/Fe_{HR} values
278 >0.7 throughout Intervals 1b, 2, and 3.

279 Changes in the trace metal inventory of the ocean, particularly within a partially restricted
280 basin, could affect interpretation of trace metal redox proxies. Low Mo/TOC values in the
281 Niobrara Formation relative to modern marine sediments indicate significant basin restriction
282 and/or a reduced global Mo seawater budget (Tessin et al., 2015). However, variability in the
283 Mo/TOC record, specifically higher Mo/TOC values coeval with elevated Mo and TOC
284 concentrations, suggests that Mo is not being forced by changes in the Mo budget of the ocean
285 (Fig. 3). Additionally, the consistency of trends across all trace metals, paired with biological
286 evidence, demonstrates that the trace metal distributions are likely primarily controlled by redox
287 conditions. Therefore, the lack of variability in Fe_{py}/Fe_{HR} values suggests that this proxy may
288 have been insensitive to redox fluctuations displayed by trace metal enrichments during and after
289 OAE 3 in the WIS (Fig. 6).

290 The disagreement between the trace metal distributions and the Fe speciation could be
291 explained by either significant porewater sulfidization of reactive Fe or downward moving
292 sulfidization fronts. Elevated TOC concentrations during Intervals 2 and 3 indicate a significant
293 increase in organic matter flux to the sediments, which would result in elevated sedimentary
294 sulfate reduction, increased porewater H_2S concentrations, and enhanced porewater sulfidization
295 of reactive Fe. While it is generally assumed that water column sulfide is required to scavenge
296 Fe^{2+} and produce elevated Fe_{py}/Fe_{HR} and Fe_{HR}/Fe_T ratios, a recent study from the Peel-Harvey
297 Estuary in Australia illustrated that significant Fe sulfidization in sediments can occur despite

298 deposition under a <2m deep, oxic water column (Kraal et al., 2013). The Peel-Harvey estuary
299 sediments similarly exhibit large Fe_{HR} enrichments despite the absence of an anoxic water
300 column. Efficient Fe sulfidization has also been recorded within the surface sediments of the
301 highly productive Achterwasser lagoon in the SW Baltic Sea, despite oxic conditions at the
302 sediment-water interface (Neumann et al., 2005). These observations of significant early
303 diagenetic sulfidization of reactive Fe within the surface sediments of modern sites support the
304 possibility of pore water, rather than water column, sulfidization of reactive Fe within the WIS.
305 Downward moving sulfidization fronts associated with peak export productivity during
306 Intervals 2a and 2c could also have pyritized reactive Fe deposited in the underlying Intervals 1b
307 and 2b. Trace metal and TOC results indicate that sediments in Intervals 1b and 2b were
308 deposited under conditions characterized by enhanced oxygenation and/or reduced export
309 productivity. Enhanced levels of sulfate reduction under elevated export productivity during
310 Intervals 2a and 2c could have led to porewater H_2S accumulation (for example, around a
311 sulfate-methane transition zone), which could "burn down" into underlying organic- and Fe-
312 poor sediments, sulfurizing any available Fe_{HR}. Diagenetic sulfidization of reactive Fe in
313 sediments underlying high TOC sediments has been recorded in a number of modern settings
314 including the Black Sea, Kau Bay, and the Arabian Sea OMZ (Neretin et al., 2004; Middelburg,
315 1991; Schenau et al., 2002) and also occurred below Mediterranean sapropels (Passier et al.,
316 1996). These sulfidization processes occur far below the sediment-water interface, and are not
317 associated with any OC or trace metal enrichments, which could explain the discrepancy
318 between trace metal, TOC, and Fe results within Intervals 1b and 2b.
319 Reactive Fe consumption within sediments, whether through early diagenetic
320 sulfidization near the surface sediment or through post-depositional sulfide burn down, could

occur more readily under low Fe availability. Despite elevated Fe_{HR}/Fe_T ratios, the Fe_T/Al record rarely shows Fe enrichments after Intervals 1a (Fig. 2). A marked increase in Fe_T/Al during Interval 2a (up to 0.88) and a more modest increase during Interval 2c (up to 0.58) paired with elevated Fe_{HR}/Fe_T and Fe_{py}/Fe_{HR} values (>0.38; >0.7) are consistent with pyrite formation in a euxinic water column. In general, however, the majority of Fe_T/Al ratios from Intervals 1b to 3 are below the average shale value of 0.55, strongly supporting that Fe could be the limiting pyrite formation in the WIS.

Although Fe_T/Al values are relatively low, a significant portion of this Fe is Fe_{HR}. Potential sources of reactive Fe to the deep basin of the WIS include Fe shuttled from the shallower to the deeper parts of the basin, the influx of nutrient-rich Tethyan water to the WIS during the Niobrara transgression, and Fe associated with volcanic ash. Regardless of the relative influence of these Fe sources, Fe_T/Al ratios generally suggest that, especially during Intervals 1b, 2b, and 3, Fe delivery to the sediments is low, which could promote porewater sulfide accumulation and reactive Fe consumption. While Fe speciation has not been measured elsewhere in the WIS during OAE 3, in depth analysis of Fe-S-C relationships in the Berthoud State #4 core indicated that, similar to the Portland core, pyrite formation was reactive Fe limited during deposition of the Niobrara Formation (Dean and Arthur, 1989; Fig. 1). Furthermore, average Fe_T/Al ratios within the Berthoud and the Aristocrat Angus cores are 0.39 and 0.38, respectively, within the Niobrara subunits that are equivalent to our OAE and post-OAE intervals (Dean and Arthur, 1998; Locklair et al., 2011; SI Table 2; Fig.1). Ratios of Fe_T/Al below crustal values (0.55) at all three sites support the conclusion that low Fe delivery was a persistent phenomenon throughout the deep basin in central Colorado during and after OAE 3. Efficient Fe retention in shallower, nearshore sediments due to expansion of sedimentary sulfidic conditions

could limit Fe shuttling, reducing the supply of reactive Fe to the deepest regions of the WIS. Recent work by Scholz et al. (2014) demonstrates that a relatively narrow window of redox conditions that promote Fe release exists, such that slightly more reducing conditions on the "shelf" could limit Fe supply to the deepest portions of the basin.

Our results suggest that Fe limitation, paired with either elevated early diagentic sulfidization of reactive Fe in surface sediments or downward moving sulfidization fronts, can lead to significant porewater pyrite formation, suggesting that particular attention should be taken when applying the Fe_{py}/Fe_{HR} proxy to reconstruct water column redox at sites characterized by low Fe availability and elevated export productivity.

Implications of low Fe availability

The ability of Fe to buffer porewater sulfide has been proposed as a mechanism to decrease organic matter preservation in sediments (e.g. Meyers et al., 2005; Meyers, 2007; Tribovillard et al., 2015). When reactive Fe is readily available, it can buffer porewater H_2S accumulation via Fe-sulfide formation. Conversely, when reactive Fe is limited, H_2S can accumulate in porewaters more rapidly (Meyers et al., 2005). Resulting high porewater H_2S concentrations create inhospitable conditions for infauna and, subsequently, can reduce the degree of bioturbation (Meyers et al., 2005; Meyers 2007). A reduction in bioturbation and bioirrigation, in turn, influences the composition of the porewater and solid constituents in sediments because infaunal organisms ventilate the substrate with oxygen-rich waters, stimulating microbial activity and reducing sedimentary organic matter preservation (Aller, 1978; Kristensen, 2000; Zonneveld et al., 2010).

366 During the Coniacian-Santonian, a strong relationship is found between S concentrations,
367 bioturbation-derived IOC, and TOC in the Portland core (Fig. 4). Interval 1a is highly
368 bioturbated and characterized by low TOC, indicating that burrowing organisms and the
369 associated oxidative processes resulted in near complete OC loss from the sediments. When
370 oxygen limitation reduces macrofaunal activity, beginning at the end of Interval 1, the reduction
371 in bioturbation reduced sedimentary ventilation and oxygen exposure time. The increase in
372 Fe_{py}/Fe_{HR}, S_{excess}/TS, and TS/Al ratios near the end of Interval 1 (Figure 2) suggests that a
373 drawdown of reactive Fe by H_2S consumption is coeval with the observed onset of reduced
374 benthic activity. Coeval changes in Hydrogen Index and Oxygen Index (HI and OI) values
375 indicate enhanced preservation of hydrogen-rich, oxygen-poor organic matter in laminated or
376 microbioturbated sediments. These combined results support that a reactive Fe limitation led to
377 increased porewater sulfide concentrations, reduced bioturbation and bioirrigation, and increased
378 organic matter preservation. Changes in organic matter composition (HI and OI) occur alongside
379 significant increases in measured TOC concentrations, highlighting the importance of changes in
380 organic matter preservation during periods of enhanced OC burial.
381 Another consequence of a reactive Fe limitation is the possible sulfurization of organic
382 matter (Zaback et al., 1993; Meyers, 2007; Tribovillard et al., 2015). Organic matter
383 sulfurization occurs when excess sulfide (not reacted with Fe) modifies organic matter functional
384 groups, such as lipids and carbohydrates. During and after OAE 3, 20–45% of S is in excess of
385 pyrite S and S_{excess} generally tracks TOC, indicating that excess S may be associated with organic
386 matter accumulation (Fig. 4). Sulfurization would make organic matter more resistant to
387 degradation, further promoting organic matter preservation throughout Intervals 2 and 3.

By reducing sedimentary P sequestration (the so called "Phosphorus Trap"), an Fe limitation could also directly impact nutrient recycling within sediment porewaters, helping to sustain elevated levels of primary production throughout the prolonged interval of black shale deposition. Iron speciation is known to control benthic P recycling and can therefore impact the return of nutrients buried with organic matter to the photic zone. Generally, as organic matter degrades in surface sediments, phosphate (PO_4^{3-}) is released to porewaters where it can be adsorbed on Fe oxyhydroxides, providing an efficient sedimentary sink for P. However, under O_2 depleted conditions, Fe oxyhydroxides are dissolved and thus, P adsorption is limited (Rozan et al., 2002). In the presence of free H_2S, Fe will precipitate as Fe-sulfides (e.g. FeS and FeS_2), which have a low affinity for PO_4^{3-} (Krom and Berner, 1980). Enhanced P recycling in the presence of sulfide has been suggested as a means to sustain primary productivity (Van Cappellen and Ingall, 1994), indicating that a change in how nutrients are recycled from the sediments could be as important as changes in external nutrient input for nutrient dynamics and primary productivity in the WIS.

Elevated P/Al and low TOC/P values during Interval 1 indicate P sequestration in sediments. Conversely, during Intervals 2 and 3, P/Al values decrease and TOC/P values increase suggesting that P is no longer efficiently sequestered in the sediments (Fig. 5). Changes in P burial are coeval with increased pyrite abundance and low siderite, magnetite, and Fe (oxyhydr)oxides abundances (Figure 2), indicating that increased sedimentary P release is caused by Fe sulfidization. Our results support enhanced P recycling during the OAE and post-OAE intervals because (1) TOC/P records are consistently elevated during Intervals 2 and 3, as compared to Interval 1, and (2) P/Al ratios are very low compared to average shale values,

410 despite significant increases in organic matter deposition during Intervals 2 and 3, which would
411 deliver P to the sediments.
412
413 *Implications for the development of OAEs*
414 Elevated Fe delivery was proposed to be a primary control on low OC accumulation within
415 the WIS during OAE 2 by reducing organic matter preservation and enhancing sedimentary
416 phosphate burial (Meyers, 2007). Our results indicate that, during OAE 3, Fe cycling had the
417 opposite effect and promoted prolonged black shale deposition both during and after the OAE.
418 Efficient organic matter preservation and P recycling during the Coniacian-Santonian could
419 provide a feedback mechanism that explains the prolonged duration of black shale deposition
420 during OAE 3 within the WIS as compared to OAE 2.
421 The role of P release from sediments during Cretaceous OAEs has been the focus of recent
422 work in other ocean basins. Geochemical evidence of enhanced sedimentary P recycling during
423 OAE 2 has been found from the Tethys, WIS, and proto-Atlantic Ocean (Mort et al., 2007;
424 Tsandev and Slomp, 2009; Kraal et al., 2010). Furthermore, the termination of OAE 2 is
425 associated with an increase in sedimentary P sequestration, indicating that P burial was a
426 possible control on the duration of the event (Kraal et al., 2010). Conversely, sustained
427 sedimentary P recycling in the WIS could have prolonged OC burial after the OAE 3 interval if
428 remineralized P was returned to the photic zone.
429 Phosphorus recycling in the WIS appears to be distinct from the Proto-Atlantic during OAE
430 3. Previous work on OAE 3 from the Demerara Rise indicated that fluctuating ferruginous and
431 euxinic conditions caused periods of massive P deposition that probably decreased levels of
432 primary productivity (März et al., 2008). While the samples in our study were collected at a

lower resolution than the Demerara Rise study, our results do not provide similar evidence of P burial during OAE 3, even during better oxygenated periods such as Interval 2b. Specifically, the new results indicate that reactive Fe, not sulfate, was consistently limiting within the WIS throughout Intervals 1b, 2, and 3, thereby, inhibiting P burial throughout OAE 3 and afterwards. The ferruginous/euxinic fluctuations observed at the Demerara Rise, but not the WIS, could be attributed to either periodic influence of oxic South Atlantic water masses at the Demerara Rise or sulfate drawdown in the restricted Proto-Atlantic (März et al., 2008).

Similar ferruginous/euxinic redox fluctuations associated with variable continental Fe delivery were observed in OAE 2 deposits from Tarfaya, Morocco; however, efficient P recycling was also observed throughout OAE 2 (Poulton et al., 2015). Further detailed and high-resolution geochemical work is, therefore, necessary to look for relationships between Fe speciation and enhanced P recycling at other Cretaceous sites that experienced prolonged periods of black shale deposition. Additionally, the relationship between changes in organic matter composition, bioturbation and Fe speciation should be determined during OAEs to evaluate whether an Fe limitation was important to OAE development in other regions, or only within the WIS.

Conclusions

Iron speciation results from OAE 3 suggest that a reactive Fe limitation may have stimulated and maintained enhanced OC burial after the initial development of anoxia within the WIS by increasing organic matter preservation in sediments and enhancing nutrient recycling. Preceding the onset of increased OC burial, Fe speciation results record a shift from predominantly non-sulfide Fe phases (carbonate, (oxyhydr)oxides, and magnetite) to

predominantly sulfide Fe phases. Intervals 2 and 3 are characterized by stable, elevated pyrite formation despite other proxies recording significant redox variability, suggesting efficient Fe sulfidization, either within surface sediments or due to downward migration of sulfidization fronts. Significant sulfidization of Fe, paired with low Fe_T/Al ratios, indicates that reactive Fe may be limiting sedimentary pyrite formation.

Our results highlight two complications for using Fe as a redox proxy on geologic timescales: (1) similar to modern observations, reactive Fe is sequestered in early diagenetic carbonate phases during Interval 1a producing anomalously elevated Fe_T/Al values independent of redox conditions, and (2) efficient sulfidization of reactive Fe within the Fe-limited WIS, obscured redox variability before, during and after the OAE.

A reactive Fe limitation could promote organic matter preservation in sediments because the amount of reactive Fe was insufficient to buffer porewater H_2S concentrations through Fe-sulfide formation. Coeval changes in Fe, S, bioturbation and organic matter composition support that changes in Fe availability reduced the sedimentary "sulfide buffer," reducing bioturbation and producing conditions more conducive to organic matter preservation. During Interval 1a, the availability of non-sulfide Fe phases promoted P sequestration. However, as porewater H_2S accumulation increased, sulfidization of reactive Fe phases promoted P release from the sediments. This change in phosphate cycling could have prolonged enhanced OC burial during and after OAE 3 by stimulating enhanced primary productivity in the WIS, helping to extend the duration of OAE 3 as compared to OAE 2.

Distinct C-S-P cycling in the WIS during the Coniacian-Santonian, as compared to the Proto-Atlantic, during supposedly stable and widespread anoxic periods in the Late Cretaceous oceans, indicates that there was a significant amount of spatial variability between open shelf

479 settings, continental margins, and epicontinental seas such as the WIS. Detailed studies of
480 stratigraphically equivalent sediment intervals in high resolution, using a range of
481 sedimentological and geochemical tools will enable a more complete understanding of the
482 biogeochemical cycles of the Cretaceous greenhouse ocean.
483
484 **Acknowledgements**
485
486 We would like to thank Danielle Boshers for assistance with sample processing and Aurélie
487 Dhenain for analytical support. We are grateful to the USGS Core Research Center for sample
488 collection. This work was supported by ACS-PRF grant (#53845-ND8) to NDS and IH and a
489 Scott Turner Award from the Department of Earth and Environmental Sciences at UM. AT was
490 supported by an NSF-GRF (DGE 1256260). ACS-PRF 54583-DNI2 and NSF-EAR 1503596
491 provided funding for AC. An earlier version of this paper was improved by reviews by reviews
492 from Stephen Meyers, Christian März, and two anonymous reviewers.

493

494 **REFERENCES**

495 Algeo, T., E. Ingall (2007), Sedimentary C_{org}:P ratios, paleocean ventilation, and Phanerozoic
496 atmospheric O_2, *Palaeogeography Palaeoclimatology Palaeoecology 256*, 130-155.

497 Algeo, T., J.B. Maynard (2004), Trace-element behavior and redox facies in core shales of Upper
498 Pennsylvanian Kansas-type cyclothems, *Chemical Geology, 206*, 289-318.

499 Anderson, TF, Raiswell, R (2004) Sources and mechanisms for the enrichment of highly reactive
500 iron in euxinic Black Sea sediments , *American Journal of Science*, *304*, 203-233.

501 Arthur, M. A., S.O. Schlanger, and H.C. Jenkyns (1987), The Cenomanian-Turonian Oceanic
502 Anoxic Event, II, Paleoceanographic controls on organic matter production and
503 preservation, in Marine Petroleum Source Rocks, Geological Society of London Special
504 Paper, edited by J. a. A. F. Brooks, pp. 401-420.
505
506 Boyd, P. W., et al. (2000), A mesoscale phytoplankton bloom in the polar Southern Ocean
507 stimulated by iron fertilization, *Nature, 407*, 695-702.
508
509 Canfield, D.e. (1989), Reactive iron in marine sediments, *Geochimica et Cosmochimica Acta,*
510 *53*, 619-623.
511
512 Canfield DE, Raiswell R, Westrich JT, Reaves CM, Berner RA (1986), The use of chromium
513 reduction in the analysis of reduced inorganic sulfur in sediments and shales, *Chemical*
514 *Geology 54*,149–155.
515
516 Chappaz, A., T. Lyons, D. Gregory, C. Reinhard, B. Gill, C. Li, R. Large (2014), Does pyrite act
517 as an important host for molybdenum in modern and ancient sediments?, *Geochimica et*
518 *Comsmochimica Acta, 126*, 112-122.
519
520 Clarkson, M., S. Poulton, R. Wood, R. Guilbaud (2014), Assessing the utility of Fe/Al and Fe-
521 speciation to record water column redox conditions in carbonate-rich sediments,
522 *Chemical Geology 382*, 111-122.
523
524 Crusius, J., S. Calvert, T. Pedersen, and D. Sage (1996), Rhenium and molybdenum enrichments
525 in sediments as indicators of oxic, suboxic and sulfidic conditions of deposition, *Earth*
526 *and Planetary Science Letters, 145*(1-4), 65-78.
527
528 Dean, W.E., M. A. Arthur (1989), Iron-sulfur-carbon relationships in organic-carbon-rich
529 sequences: Cretacesou Western Interior Seaway, American Jounal of Science, 289 (6),
530 708-743.
531
532 Dean, W. E., M. A. Arthur (1998), Geochemical expressions of cyclicity in Cretaceous pelagic
533 limestone sequences: Niobrara Formation, Western Interior Seaway, in *Stratigraphy and*

534 *Paleoenvironments of the Cretaceous Western Interior Seaway*, edited by W. E. a. M. A.
535 A. Dean, pp. 227-255, SEPM Concepts in Sedimentology and Paleontology.
536
537 Erickson BE, Helz GR (2000), Molybdenum (VI) speciation in sulfidic waters: Stability and
538 lability of thiomolybdates, *Geochimica et Cosmochimica Acta, 64*, 1149-1158

539 Fernex, F., Février, G., Benaïm, J., Arnoux, A. (1992), Copper, lead and zinc trapping in
540 Mediterranean deep-sea sediments: probable coprecipitation with manganese and iron,
541 *Chemical Geology, 98*, 293–308.

542 Floegel, S., W. W. Hay, R. M. DeConto, and A. N. Balukhovsk (2005), Formation of
543 sedimentary bedding couplets in the Western Interior Seaway of North America -
544 implications from climate system modeling, *Palaeogeography Palaeoclimatology*
545 *Palaeoecology 218*(1-2), 125-143.

546 Hattin, D.E., 1982. Stratigraphy and depositional environment of Smoky Hill Chalk Member,
547 Niobrara Chalk (Upper Cretaceous) of the type area, Western Kansas. Kansas Geological
548 Society Bulletin 225, 108 p.

549 Huerta-Diaz, M.A., Morse, J.W. (1992), Pyritisation of trace metals in anoxic marine sediments,
550 *Geochimica et Cosmochimica Acta, 56*, 2681–2702.

551 Jenkyns, H. C. (2010), Geochemistry of oceanic anoxic events, *Geochemistry Geophysics*
552 *Geosystems*, *11*.

553 Kraal, P., E. Burton, R. Bush (2013), Iron monosulfide accumulation and pyrite formation in
554 eutrophic estuarine sediments, *Geochimica et Cosmochimica Acta, 122*, 75-88.
555
556 Kraal, P., C. P. Slomp, A. Forster, M. M. M. Kuypers (2010), Phosphorus cycling from the
557 margin to abyssal depths in the proto-Atlantic during oceanic anoxic event 2,
558 *Palaeogeography, Palaeoclimatology, Palaeoecology 295* (1), 42-54.
559
560 Krom, M., R. Berner (1980), Adsorption of phosphate in anoxic marine sediments, *Limnology*
561 *and Oceanography, 25*(5), 797-806.
562
563 Locklair, R., B. Sageman, and A. Lerman (2011), Marine carbon burial flux and the carbon
564 isotope record of Late Cretaceous (Coniacian-Santonian) Oceanic Anoxic Event III,
565 *Sedimentary Geology 235*(1-2), 38-49.

566 Lyons TW, Severmann S (2006), A critical look at iron paleoredox proxies: new insights from
567 modern euxinic marine basins, *Geochimica Et Cosmochim Acta 70*, 5698–5722

568 März, C., S. W. Poulton, B. Beckmann, K. Kuester, T. Wagner, and S. Kasten (2008), Redox
569 sensitivity of P cycling during marine black shale formation: Dynamics of sulfidic and
570 anoxic, non-sulfidic bottom waters, *Geochimica Et Cosmochimica Acta*, *72*(15), 3703-
571 3717.

572 Meyers, S.R., Sageman, B.B., and Lyons, T. (2005), Organic carbon burial rate and the
573 molybdenum proxy: Theoretical framework and application to Cenomanian-Turonian
574 OAE II, *Paleoceanography*, PA2002, doi:10.1029/2004PA001068.

575 Meyers, S.R. (2007), Production and preservation of organic matter: The significance of iron:
576 *Paleoceanography 22*, PA4211, doi:10.1029/2006PA001332.

577 Middelburg, J. (1991), Organic carbon, sulfur, and iron in recent semi-euxinic sediments of Kau
578 Bay, Indonesia, *Geochimica et Cosmochimica Acta 55*, 815-828.

579 Neretin, L., M. Bottcher, B. Jorgensen, I. Volkov, H. Luschen, K. Hilgenfeldt (2004),
580 Pyritization processes and greigite formation in advancing sulfidization front in the
581 Upper Pleistocene sediments of the Black Sea, *Geochimica et Cosmochimica Acta 68*(9),
582 2081-2093.

583 Neumann, T., N. Rausch, T. Leipe, O. Dellwig, Z. Berner, M. Bottcher (2005), Intense pyrite
584 formation under low-sulfate conditions in the Achterwasser lagoon, SW Baltic Sea,
585 *Geochimica et Cosmochimica Acta 69*(14), 3619-3630.

586 Mort, H. P., T. Adatte, K. B. Follmi, G. Keller, P. Steinmann, V. Matera, Z. Berner, and D.
587 Stuben (2007), Phosphorus and the roles of productivity and nutrient recycling during
588 oceanic anoxic event 2, *Geology 35,* 483–486.

589 Passier, H., J. Middelburg, B. van Os, G. De Lange (1996), *Geochimica et Cosmochimica Acta*
590 *60*(5), 751-763.
591
592 Piper, D.Z., Perkins, R.B. (2004), A modern vs. Permian black shale— the hydrography, primary
593 productivity, and water-column chemistry of deposition, *Chemical Geology, 206*, 177–
594 197.
595
596 Poulton SW, Canfield DE (2005), Development of a sequential extraction procedure for iron:
597 implications for iron partitioning in continentally derived particulates, *Chemical Geology*
598 *214*, 209–221
599 Poulton, SW, Raiswell, R (2002) The low-temperature geochemical cycle of iron: From
600 continental fluxes to marine sediment deposition, *American Journal of Science*, *302,* 774-
601 805.
602
603 Poulton SW, Fralick PW, Canfield DE (2004), The transition to a sulphidic ocean 1.84 billion
604 years ago, *Nature 431*, 173–177
605
606 Poulton, S., S. Henkel, C. Marz, H. Urquhart, S. Floegel, S. Kasten, J. Sinninghe Damste, T.
607 Wagner (2015), A continental-weathering control on orbitally driven redox-nutrient
608 cycling during Cretaceous Oceanic Anoxic Event 2, *Geology, 43* (11), 963-966.
609
610 Raiswell R, Anderson TF (2005), Reactive iron enrich- ment in sediments deposited beneath
611 euxinic bottom waters: constraints on supply by shelf recycling, *Geological Society of*
612 *London Special Publications 248*, 179–194

Raiswell, R, Canfield, DE (1996) Rates of reaction between silicate iron and dissolved sulfide in Peru Margin sediments, *Geochimica et Cosmochimica Acta*, *60*, 2777-2787.

Raiswell, R; Canfield, DE (1998) Sources of iron for pyrite formation in marine sediments, *American Journal of Science*, *298*, 219-245.

Raiswell, R., Reinhardt, C.T., Derkowski, A., Owens, J., Bottrell, S.H., Anbar, A.D., Lyons, T.W. (2011) Formation of syngenetic and early diagenetic iron minerals in the late Archean Mt. McRae Shale, Hamersley Basin, Australia: new insights on the patterns, controls and paleoenvironmental implications of authigenic mineral formation. *Geochimica Cosmochimica Acta, 25*, 1072-1087.

Rozan, T, M. Taillefert, R. Trouwborst, B. Glazer, S. Ma, J. Herszage, L. Valdes, K. Price, G. Luther III (2002), Iron-sulfur-phospohorus cycling in the sediment of a shallow coastal bay: Implications for sediment nutrient release and benthic macroalgal blooms, *Limnology and Oceanography 47*(5), 1346–1354.

Sageman, B., M. Arthur (1994), Early Turonian paleogeographic/paleobathymetric map, Western Interior, US *in* Caputo, M. V., Peterson J. A., and Franczyk, K.J., eds., Mesozoic Systems of the Rocky Mountain Region, USA: SEPM, Rocky Mountain Section, 457-470.

Sageman, B. B., S. R. Meyers, M. A. Arthur (2006), Orbital time scale and new C-isotope record for Cenomanian-Turonian boundary stratotype, *Geology, 34* (2), 125-128.

Savdra, C. E. (1998), Ichnocoenoses of the Niobrara Formation: Implications for benthic oxygenation histories, in *Stratigraphy and Paleoenvironments of the Cretaceous Western Interior Seaway*, edited by W. E. a. M. A. A. Dean, pp. 227-255, SEPM Concepts in Sedimentology and Paleontology.

Schenau, S.J., Reichart, G.J. and De Lange, G.J. (2002), Oxygen minimum zone controlled Mn redistribution in Arabian Sea sediments during the late Quaternary, *Paleoceanography 17.*

Schlanger, S. O., M. A. Arthur, H. C. Jenkyns, P. A. Scholle (1987), The Cenomanian-Turonian Oceanic Anoxic Event, I. Stratigraphy and distribution of organic carbon-rich beds and the marine δ13C excursion, *Geological Society, London, Special Publications 26* (1), 371-399.

Scholz, F., J. McManus, A. Mix, C. Hensen, R. Schneider (2014), The impact of ocean deoxygenation on iron release from continental margin sediments, *Nature Geoscience 7*, 433-437.

Scott, C., and T. W. Lyons (2012), Contrasting molybdenum cycling and isotopic properties in euxinic versus non-euxinic sediments and sedimentary rocks: Refining the paleoproxies, *Chemical Geology 324*, 19-27.

Scott, G. R., and W. A. Cobban (1964), Stratigraphy of the Niobrara Formation at Pueblo, Colorado, *Professional Papers US Geological Survey*, *454-L*, L1-L30.

Severmann, S., J. McManus, W. Berelson, D. Hammond (2010), The continental shelf benthic iron flux and its isotope composition, *Geochimica et Cosmochimica Acta 74*, 3984-4004.

Tessin, A., I. Hendy, N. Sheldon, B. Sageman (2015), Redox-controlled preservation of organic matter during "OAE 3" within the Western Interior Seaway, *Paleoceanography 30* (6), 702-717.

Tribovillard, N., T. Algeo, T. Lyons, A. Riboulleau (2006), Trace metals as paleoredox and paleoproductivity proxies: an update, *Chemical Geology, 232*, 12-32.

Tribovillard, N., E. Hatem, O. Averbuch, F. Barbecot, V. Bout-Roumazeilles, A. Trentesaux (2015), Iron availability as a dominant control on the primary composition and diagenetic overprint of organic-matter-rich rocks, *Chemical Geology 401*, 67-82.

Tsandev, I., C. P. Slomp (2009), Modeling phosphorus cycling and carbon burial during Cretaceous Oceanic Anoxic Events, *Earth and Planetary Science Letters 286* (1), 71-79.

Tsikos, H., H.C. Jenkyns, B. Walsworth-Bell, M. R. Petrizzo, A. Forster, S. Kolonic, W. Erba, I. Premoli Silva, M. Baas, T. Wagner, J. Sinninghe Damste (2004) Carbon-isotope stratigraphy recorded by the Cenomanian-Turonian oceanic anoxic event: correlation and implications based on three key-localities, *Journal of the Geological Society, 161*, 711-720.

Van Cappellen P. and Ingall E (1994), Benthic phosphorus regeneration, net primary production, and ocean anoxia: A model of the coupled marine biogeochemical cycles of carbon and phosphorus, *Paleoceanography 9*, 677-692.

Wagreich, M. (2012), "OAE 3" --regional Atlantic organic carbon burial during the Coniacian-Santonian, *Climate of the Past*, *8*, 1447-1455.

Zaback, D.A., Pratt, L.M., Hayes, J.M. (1993), Transport and reduction of sulphate and immobilisation of sulphide in marine black shales, *Geology 21*, 141–144.

Zonneveld, K. A. F., et al. (2010), Selective preservation of organic matter in marine environments; processes and impact on the sedimentary record, *Biogeosciences 7*, 483–511.

Figure captions

Figure 1: (a) Map of the Cretaceous Western Interior Seaway (WIS) with Turonian paleobathymetry estimates (adapted from Sageman and Arthur, 1995). Darker colors represent relatively deeper depths. The USGS #1 Portland core location is marked with a star. Circles denote the Aristocrat Angus and Berthoud State cores. (b) Stratigraphy and total organic carbon (TOC) for the USGS Portland core with adapted intervals from Tessin et al. (2015). Gray bars denote Intervals 1b, 2b, and 3.

Figure 2: Iron concentrations and speciation results from the Portland core (a) Fe phases measured by sequential extractions (Fe_{carb}, Fe_{ox}, and Fe_{mag}), $Fe_{py,}$ and $Fe_{NR/PR}$. The thick line indicates Fe_T (wt. %). (b) Weight % ratios of Fe_T/Al. Dashed line indicates the average Fe_T/Al shale value of 0.55. (c) Fe_{HR}/Fe_T, with the anoxic threshold of 0.38 indicated by the dashed line. (d) Fe_{py}/Fe_{HR}, with the euxinic Fe_{py}/Fe_{HR} threshold of 0.7 designated by a dashed line. Gray bars denote Intervals 1b, 2b, and 3.

Figure 3: Total organic carbon (TOC) and trace metal records (Mo/Al (ppm/wt. %), Mo (ppm), Mo/TOC (ppm/wt. %), Re/Al (ppb/wt. %), Cd/Al (ppm/wt. %), and Zn/Al (ppm/wt. %)) from the USGS Portland core. Gray bars denote Intervals 1b, 2b, and 3. TOC and Mo (ppm) records are from Tessin et al. (2015).

Figure 4: Total organic carbon (TOC), Total Sulfur (TS)/Al (wt. % ratios), S_{excess}/TS, ichnofacies-derived interpreted oxygenation curve (IOC; smoothed to 0.5 m resolution), and

718 Oxygen Index and Hydrogen Index values. Gray bars denote Intervals 1b, 2b, and 3. TOC and
719 RockEval results are from Tessin et al. (2015). IOC record is adapted from Savrda (1998).
720
721 Figure 5: P/Al (weight % ratios) and TOC/P (molar ratios) records from the USGS Portland core.
722 Dashed lines indicate the average shale P/Al ratio of 0.08 and the Redfield C:P ratio of 106:1.
723 Gray bars denote Intervals 1b, 2b, and 3.
724
725 Figure 6: Crossplot of Fe_{py}/Fe_{HR} and Mo (ppm; Tessin et al. 2015). Gray circles indicate samples
726 from Interval 1; blue squares indicate samples from Interval 2 and green triangles indicate
727 samples from Interval 3. Dashed lines indicate interpreted euxinic conditions for Mo
728 concentrations (Scott and Lyons, 2012) and Fe_{py}/Fe_{HR} (März et al., 2008; Poulton and Canfield,
729 2011).
730

Figure 1

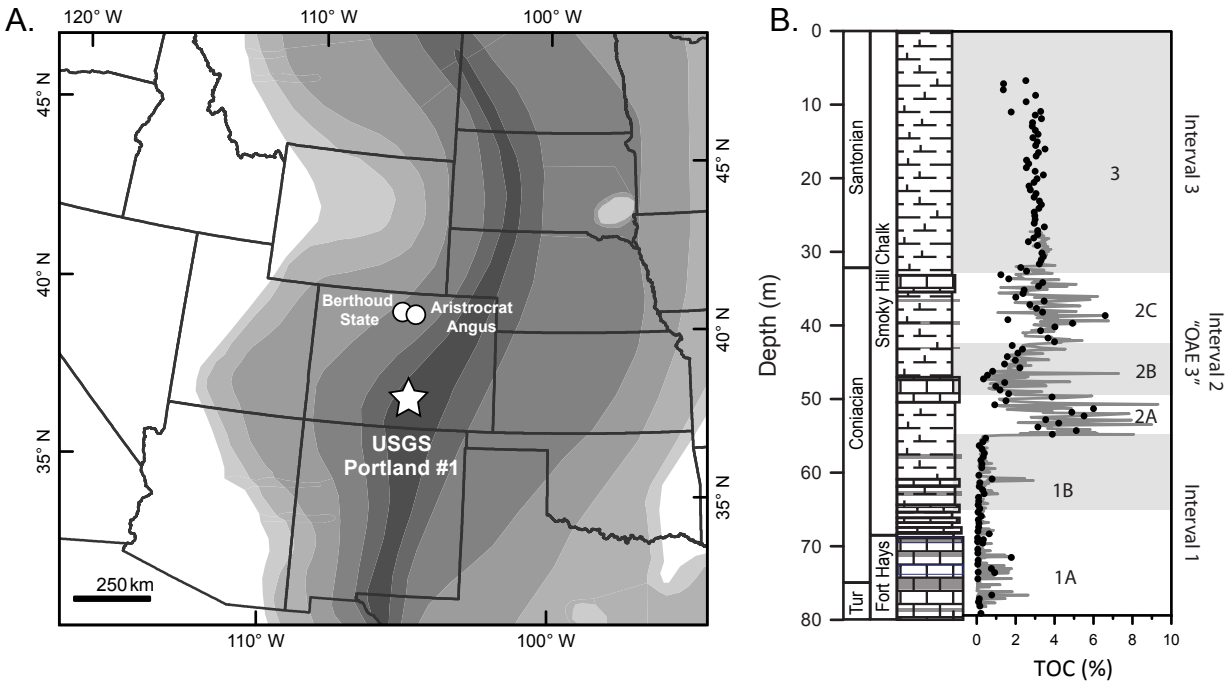
A.
120° W
110° W
100° W
45° N
40° N
35° N
Berthoud
State
Aristocrat
Angus
USGS
Portland #1
250 km
B.
Depth (m)
Santonian
Coniacian
Tur
Smoky Hill Chalk
Fort Hays
3
2C
2B
2A
1B
1A
Interval 3
Interval 2
"OAE 3"
Interval 1
TOC (%)

Figure 2

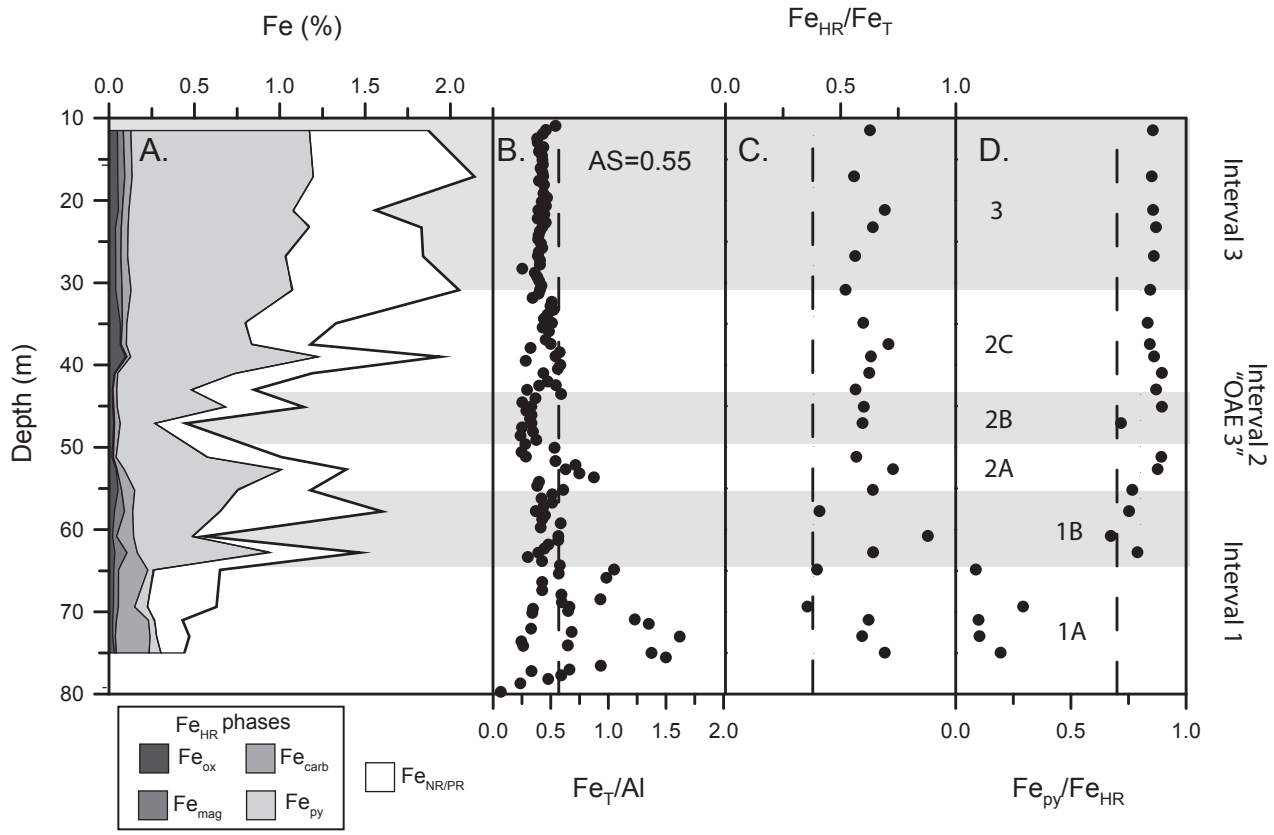
Fe (%)
Fe_{HR}/Fe_T
Depth (m)
A.
B.
AS=0.55
C.
D.
3
2C
2B
2A
1B
1A
Interval 3
Interval 2
"OAE 3"
Interval 1
Fe_{HR} phases
Fe_{ox}
Fe_{carb}
Fe_{mag}
Fe_{py}
$Fe_{NR/PR}$
Fe_T/Al
Fe_{py}/Fe_{HR}

Figure 3

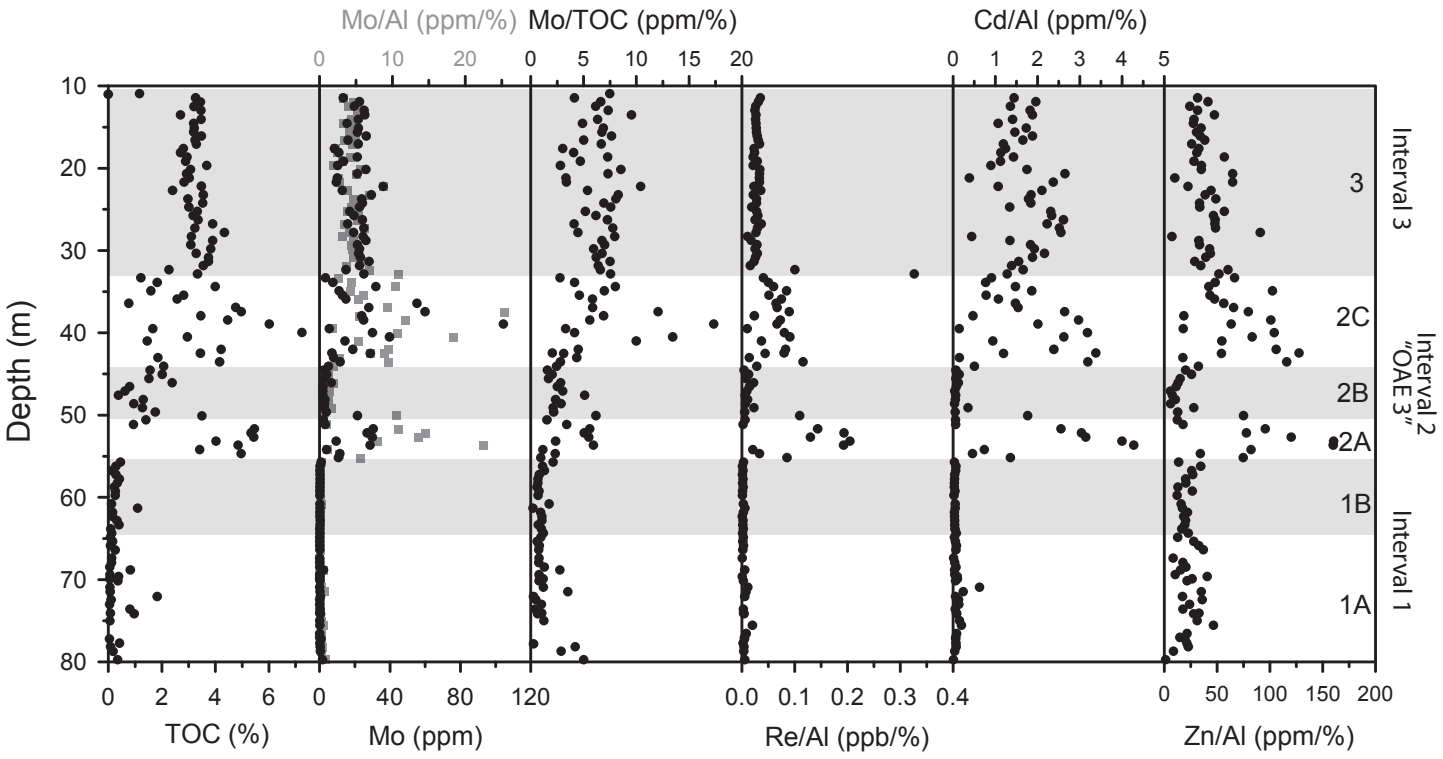
Mo/Al (ppm/%)
Mo/TOC (ppm/%)
Cd/Al (ppm/%)
Depth (m)
TOC (%)
Mo (ppm)
Re/Al (ppb/%)
Zn/Al (ppm/%)
Interval 3
3
2C
2B
2A
Interval 2
"OAE 3"
1B
Interval 1
1A

Figure 4

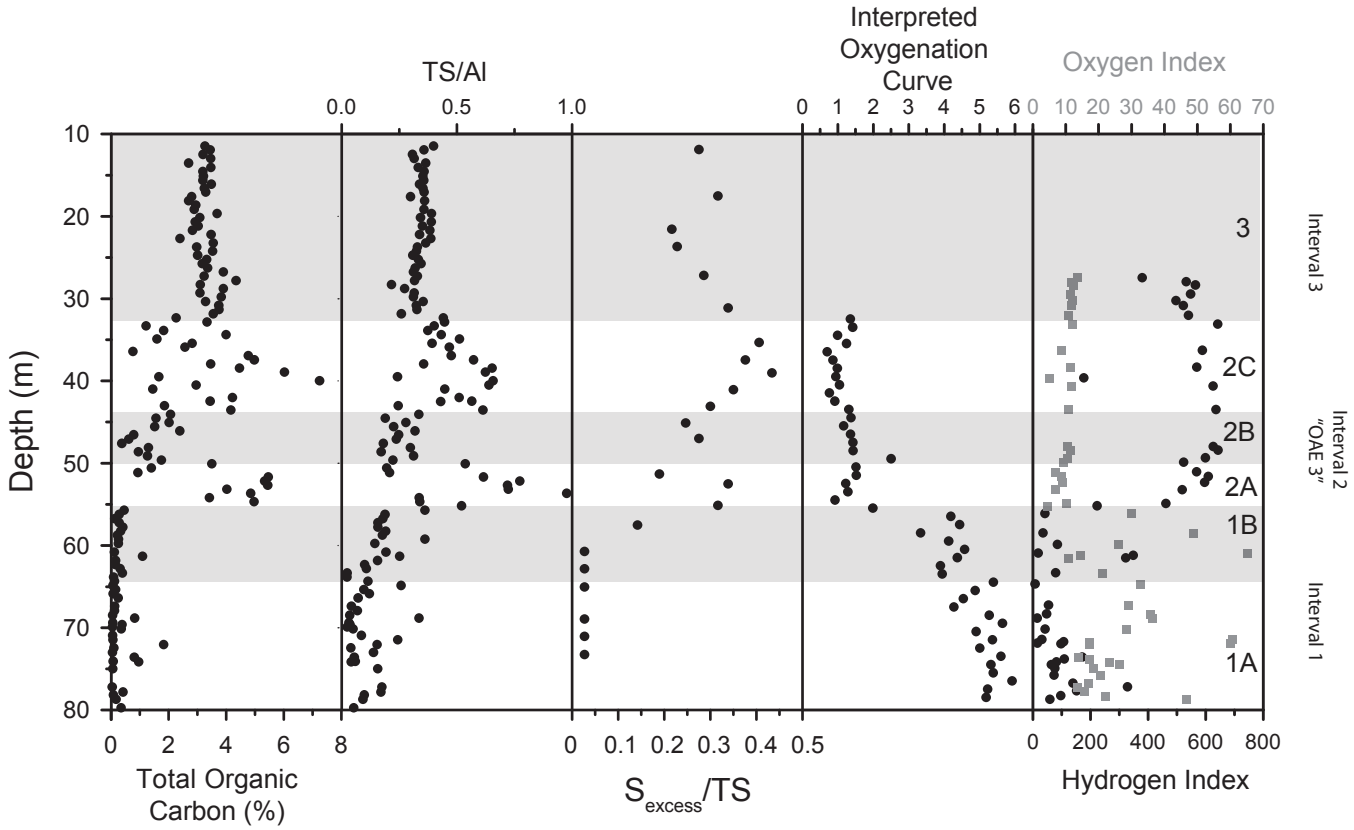
Interpreted
Oxygenation
Curve
TS/Al
Oxygen Index
Depth (m)
Total Organic
Carbon (%)
S excess/TS
Hydrogen Index
3
2C
2B
2A
1B
1A
Interval 3
Interval 2
"OAE 3"
Interval 1

Figure 5.

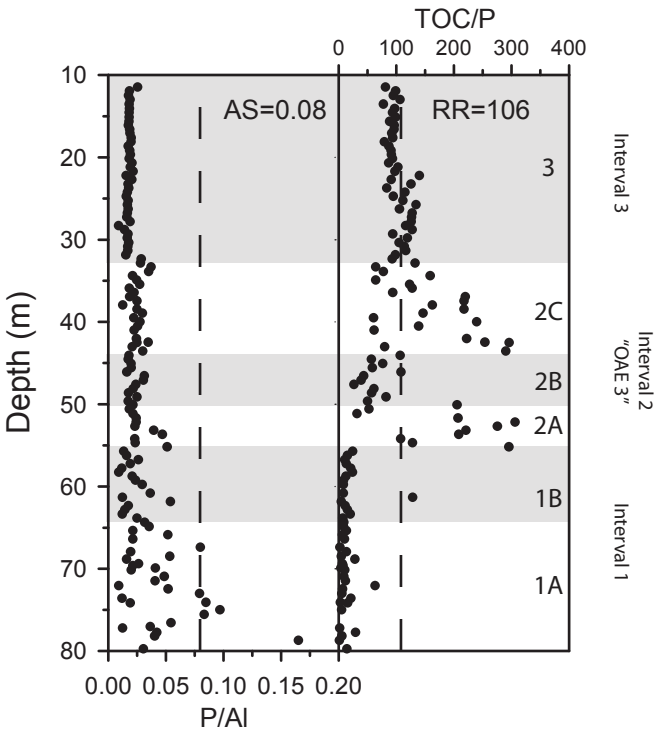
TOC/P
0
100
200
300
400
10
20
30
40
50
60
70
80
AS=0.08
RR=106
3
2C
2B
2A
1B
1A
Interval 3
Interval 2
"OAE 3"
Interval 1
Depth (m)
0.00
0.05
0.10
0.15
0.20
P/Al

Figure 6.

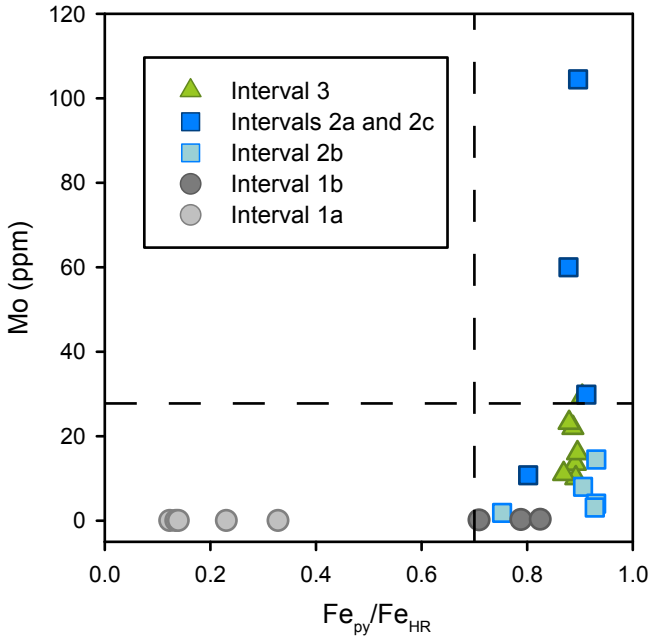
Interval 3
Intervals 2a and 2c
Interval 2b
Interval 1b
Interval 1a
Mo (ppm)
120
100
80
60
40
20
0
0.0
0.2
0.4
0.6
0.8
1.0
Fe$_{py}$/Fe$_{HR}$

Table 1: Description of iron phases and their corresponding extraction procedure adapted from März et al., 2008

Iron Phase	Extraction Procedure
Fe_{carb}: Fe bound to carbonate, including siderite and ankerite	10 mL 1 M Na-acetate (pH 4.5, shake for 48 hours)
Fe_{ox}: Fe bound as oxyhydr(oxides) including goethite and hematite	10 mL citrate-buffered Na-dithionite (pH 4.8; shake for 2 hours)
Fe_{mag}: iron bound as magnetite	10 mL Ammonium oxalate (pH 3.2; shake for 6 hours)
Fe_{tot}: total Fe including silicates	ALS procedure outlined above
Fe_{py}: Fe bound to chromium (II)-reducible sulfur	15 mL $CrCl_2$ (boiling for 2 hours; precipitated in ZnS)